Advances in Water Resources 77 (2015) 57–68

Contents lists available at ScienceDirect

Advances in Water Resources

journal homepage: www.elsevier.com/locate/advwatres

Modeling the velocity field during Haines jumps in porous media

Ryan T. Armstrong [a,*], Nikolay Evseev [c], Dmitry Koroteev [c], Steffen Berg [b]

[a] School of Petroleum Engineering, University of New South Wales, NSW, 2052 Sydney, Australia
[b] Shell Global Solutions International B.V., Kesslerpark 1, 2288 GS Rijswijk, The Netherlands
[c] Schlumberger Moscow Research, 13 Pudovkina Street, 119284 Moscow, Russia

ARTICLE INFO

Article history:
Received 16 April 2014
Received in revised form 11 January 2015
Accepted 11 January 2015
Available online 17 January 2015

Keywords:
Interfacial velocity
Haines jump
Representative elementary volume
Capillary number
Pore-scale modeling
Density functional hydrodynamics

ABSTRACT

When nonwetting fluid displaces wetting fluid in a porous rock many rapid pore-scale displacement events occur. These events are often referred to as Haines jumps and any drainage process in porous media is an ensemble of such events. However, the relevance of Haines jumps for larger scale models is often questioned. A common counter argument is that the high fluid velocities caused by a Haines jump would average-out when a bulk representative volume is considered. In this work, we examine this counter argument in detail and investigate the transient dynamics that occur during a Haines jump. In order to obtain fluid–fluid displacement data in a porous geometry, we use a micromodel system equipped with a high speed camera and couple the results to a pore-scale modeling tool called the Direct HydroDynamic (DHD) simulator. We measure the duration of a Haines jump and the distance over which fluid velocities are influenced because this sets characteristic time and length scales for fluid–fluid displacement. The simulation results are validated against experimental data and then used to explore the influence of interfacial tension and nonwetting phase viscosity on the speed of a Haines jump. We find that the speed decreases with increasing nonwetting phase viscosity or decreasing interfacial tension; however, for the same capillary number the reduction in speed can differ by an order of magnitude or more depending on whether viscosity is increased or interfacial tension is reduced. Therefore, the results suggest that capillary number alone cannot explain pore-scale displacement. One reason for this is that the interfacial and viscous forces associated with fluid–fluid displacement act over different length scales, which are not accounted for in the pore-scale definition of capillary number. We also find by analyzing different pore morphologies that the characteristic time scale of a Haines jump is dependent on the spatial configuration of fluid prior to an event. Simulation results are then used to measure the velocity field surrounding a Haines jump and thus, measure the zone of influence, which extends over a distance greater than a single pore. Overall, we find that the time and length scales of a Haines jump are inversely proportional, which is important to consider when calculating the spatial and temporal averages of pore-scale parameters during fluid–fluid displacement.

1. Introduction

For subsurface engineering applications, it is commonly understood that processes at the molecular-scale can influence field-scale results (e.g. [43]). This length-scale range, which spans 10 or more orders of magnitude, is commonly divided into the following sub-scales: molecular ($\sim 10^{-9}$ m), pore ($\sim 10^{-5}$ m), core ($\sim 10^{-3}$ m), and field (>10 m). The up-scaling of flow processes from the molecular scale to the field scale poses a challenge and is an ongoing area of research. At the pore scale, suitable averaging procedures of molecular-scale properties are used to express effective medium properties, such as, density, viscosity, and interfacial tension. This approach is similar to how the ideal gas law is obtained by ensemble averaging the multi-body statistics of non-interacting particles in a representative volume. However, the up-scaling of flow processes from the pore scale to the core scale and/or field scale is a more challenging problem. Since the 1970s, observations from pore-scale experiments have been used to identify many important displacement mechanisms, which are described by terms, such as Haines jump, snap-off, piston-like displacement, corner flow, ganglion dynamics and film swelling [5,24,34,37,38]. Sequentially, these mechanisms have been used to develop mechanistic rules for network models, as explained in Blunt [8]. Unfortunately, these concepts have no clear link to core-scale and/or field-scale models. It is neither clear what the averaging procedure from pore-scale to core-scale should be nor

* Corresponding author.

http://dx.doi.org/10.1016/j.advwatres.2015.01.008
0309-1708/

over which length scales these displacement mechanisms interact. A pore scale definition of capillary number is

$$Ca = \mu v/\sigma \quad (1)$$

where μ is viscosity, v is fluid velocity, and σ is interfacial tension. This capillary number definition is one of the key scaling groups for two-phase flow in porous media denoting the balance of viscous over capillary forces. The mobilization of capillary-trapped oil by viscous flow, i.e. capillary de-saturation [33], often occurs around a pore-scale capillary number of 10^{-5}. Dimensional analysis [28] comparing pore scale and Darcy scale immiscible displacement [28] reveals that the respective definitions of capillary number differ by the ratio of two length scales, i.e. the length scale defining the viscous forces (the length over which a viscous pressure drop is defined) and capillary forces which are not identical. Consistency can be achieved when the length of non-wetting phase clusters is taken as the length scale defining the viscous forces [3]. Oil clusters typically extend over multiple pores and can be nowadays imaged directly with fast X-ray computed tomography under dynamic flow conditions [7].

Given this complication, standard core-scale or field-scale models are often developed from empirical relationships using parameters that are easily measured in core-plug laboratory experiments [18]. While this phenomenological approach gives reasonable results for simple systems it provides no way to understanding the interconnectivity of system behavior across multiple length scales. In the last two decades, new models have been developed that provide a clearer link between the pore-scale and core-scale, e.g. [21,22,25,39]. These new models use pore-scale parameters, such as, interfacial area and curvature, contact angle, and interfacial velocity, which are volume averaged to equivalent core-scale values that are then input parameters. In this way, the larger-scale models have a clear link to the fundamental pore-scale physics rather than relying on phenomenological relationships and mechanistic observations.

Recent advances in the imaging of pore-scale displacements [3,7] and pore-scale simulations [32] can assist in understand pore-scale processes, interactions between processes, and the associated length and time scales. A wide range of multiphase flow processes can be modeled by performing pore-scale simulations on digital rock images (e.g. [11,32,35]) or using pore-network models (e.g. [19,30,42]). Methods for pore-scale simulation range from energy-based models (e.g. density functional hydrodynamics) to lattice Boltzmann models (e.g. color fluid model) to more traditional computational fluid dynamic models (e.g. volume of fluid method). For a comprehensive review on pore-scale imaging and modeling refer to Blunt et al. [9]. Complementary to simulations, new experimental techniques utilizing quasi-2D micromodel systems and high-speed photography can be used to measure pore-scale interfacial parameters, e.g. [2,36]. Fluid-fluid displacement processes can also be visualized in 3D using dynamic X-ray computed microtomography (μCT) and the resulting images can be used to measure interfacial areas and curvatures [4,7]. These developments do not only provide a way to validate numerical models. More importantly, by using fast imaging techniques and direct simulations in a complementary mode, a parameter space larger than previously attainable can be explored, information not obtainable with a single approach can be extracted, and pore-scale parameters and equivalent macro-scale parameters can be measured simultaneously.

To solve the up-scaling problem the first steps are to identify the pore-scale components that a multiphase system comprises and parameters that characterize these components, and then to study the evolution of these parameters. At the pore scale, a 3-phase system consists of two immiscible phases, a solid phase, the interfaces between phases, and a common curve formed by the intersection of all three phases. Of these components, the fluid–fluid interface can be characterized by measuring its interfacial area, which can then be up-scaled by calculating the specific interfacial area per representative volume (a^{nw}). Hassanizadeh and Gray [25] introduced a^{nw} as a missing parameter for understanding the relationship between capillary pressure (P^c) and wetting phase saturation (S^w). Since then, it has been shown by numerous researches that by including a^{nw} in the P^c-S^w relationship the hysteresis that is observed during drainage and imbibition experiments can be reduced (e.g. [10,27,30,31,40,41,42]). More recent, Gray and Miller [23] propose an approach to account for dynamic effects in capillary pressure that considers subscale variation in thermodynamic properties rather than considering local equilibrium. In their work, the assumption of local equilibrium reduces the P_c (non-equilibrium equation) to an equation where dynamic effects are explained by only the time derivative of saturation and a relaxation term, e.g. this is more aligned with the work presented by [26] and provides some contrast between common assumptions. The addition of time derivatives or other driving forces into the capillary pressure definition presumably accounts for disequilibrium at the pore-scale during flow and is likely specific to a given problem and set of assumptions. From an engineering application-based perspective, the practical implications of the disequilibrium correction remain unclear since many other unknowns, e.g. geological uncertainties in petroleum exploration, will likely dominate the solution. However, it is clear that fundamentally a formulation to account for disequilibrium is required since a relationship between the pressure difference between the non-wetting and wetting phase and the capillary pressure at an interface is unknown for dynamic conditions. In some cases, this disequilibrium (the difference between capillary pressure and phase pressure difference) is refereed to as "dynamic capillary pressure" and is known to be a rate dependent effect [44]. For example, Hilpert [29] used this rate dependent effect to model saturation overshoot at an infiltration front.

The movement of a macroscopic displacement front during drainage is an ensemble of high-speed pore-scale events, often referred to as Haines jumps. Using acoustic measurements these drainage events (Haines jumps) have been identified to occur at the millisecond time scale [14] and have been described to occur as avalanche-like events [36]. In a previous publication, we have shown that individual pore drainage events occur at an intrinsic rate, which is independent of bulk flow rate [2] and that stable displacement, for our micromodel experiments, only occurred once the bulk flow rate was greater than the intrinsic rate. While flow rate is specific to the experimental setup and thus is not a well-defined variable, the experiments demonstrate the importance of the intrinsic rate of individual pore-drainage events. Also, interfacial velocities were found to depend on local capillary pressure differences, which dependent on fluid spatial configuration at the onset of a drainage event. These findings provide evidence that pore drainage events are a non-local process that depend on bulk fluid spatial configuration and that the intrinsic rate at which pores drain influences the macroscopic displacement front. These are important points because the relevance of these pore-scale events for larger scale models is often questioned. It could be argued that the high-speed local velocities during a Haines jump would average-out for a bulk system and thus, can be neglected. However, in our opinion the problem has not yet been explored to the level or rigor necessary to make such an argument. For example, measurements of the velocity field during a Haines jump have not been provided in the literature. Also, recent simulations results provided by Ferrari and Lunati [20] suggest that pore-scale displacement effect should be considered when up-scaling.

In this study, we investigate the transient dynamics associated with a Haines jump and link the traditional mechanistic description of a Haines jump to measureable pore-scale parameters. A micromodel system equipped with a high-speed camera is used to image interfacial dynamics during drainage and the resulting images are used to measure interfacial velocities. Many of the experimental results have been published in a previous manuscript, see Armstrong and Berg [2]. These measurements are then used to validate pore-scale simulations of Haines jumps using a modeling tool called the Direct HydroDynamic (DHD) simulator [13], the results of which also give further consistency to our experimental observations. We then use the DHD simulator to explore the influence of fluid viscosity and interfacial tension on the speed of a Haines jump because this sets a characteristic time scale for fluid–fluid displacement during drainage. To measure the characteristic length scale associated with a Haines jump, and thus, the zone over which interference could occur between simultaneous jumps, we use the DHD simulator to extract the phase velocity vectors during a Haines jump. The results provide a clearer link between a mechanistic displacement process and quantifiable pore-scale parameters that define the length and time scales of a Haines jump, which has consequences when defining a multiphase phase representative elementary volume (REV) and when performing pore-scale simulations.

2. Materials and methods

2.1. Experimental system

The experimental system was explained in Armstrong et al. [4]. For convenience, we only repeat the most relevant details. The borosilicate glass micromodel was chemically etched with a hexagonal pattern (depth = 5 μm, pore diameter = 60 μm, and neck width = 13 μm) that repeats over an entire flow field of 58 mm by 35 mm. A repeating unit of pores and throats are presented in Fig. 1. The presented REV analysis of the micromodel pattern demonstrates that an observation window of approximately 250 μm in length is required for porosity stabilization. Pore drainage events were imaged at 2000 frames per second (fps) using an inverted transmission microscope equipped with a high-speed camera. The wetting phase was Millipore water and the nonwetting phase was decane. Flow rate was controlled with a syringe pump, which allowed for constant flux boundary conditions. The experimental parameters are presented in Table 1, as Case 1. These parameters were then used in the DHD simulator to compare numerical and experimental results.

A matrix of the parameters tested with the DHD simulator is presented in Table 1. Case 1 is the baseline from which either interfacial tension, viscosity, or flux is varied. Each variable is increased or decreased from its baseline value while all other parameters remain constant. In this way, the influence of a single parameter is evaluated. Test cases that are equivalent in terms of capillary number ($Ca = u v/\sigma$; where, u is viscosity, v is fluid velocity, and σ is interfacial tension) are not equivalent in terms of the independent parameters (interfacial tension, viscosity, and flux). Case 8 has the same fluid properties and boundary flux as Case 1 (baseline); however, the geometry of the porous pattern was varied. For this case, a hexagonal pattern of Gaussian distributed pore radii (mean diameter = 60 μm, range ± 20 μm) and neck widths (mean neck width = 21 μm, range ± 8 μm) were used. Also, it should be noted that the velocity used in this manuscript is the Darcy velocity calculated by considering the injection flux and the cross-sectional area of the micromodel, i.e. not just the void volume.

Interfacial velocities for both the simulation and experimental data were measured with Tracker Open Source Physics software. For the interfacial velocity analysis we have selected random

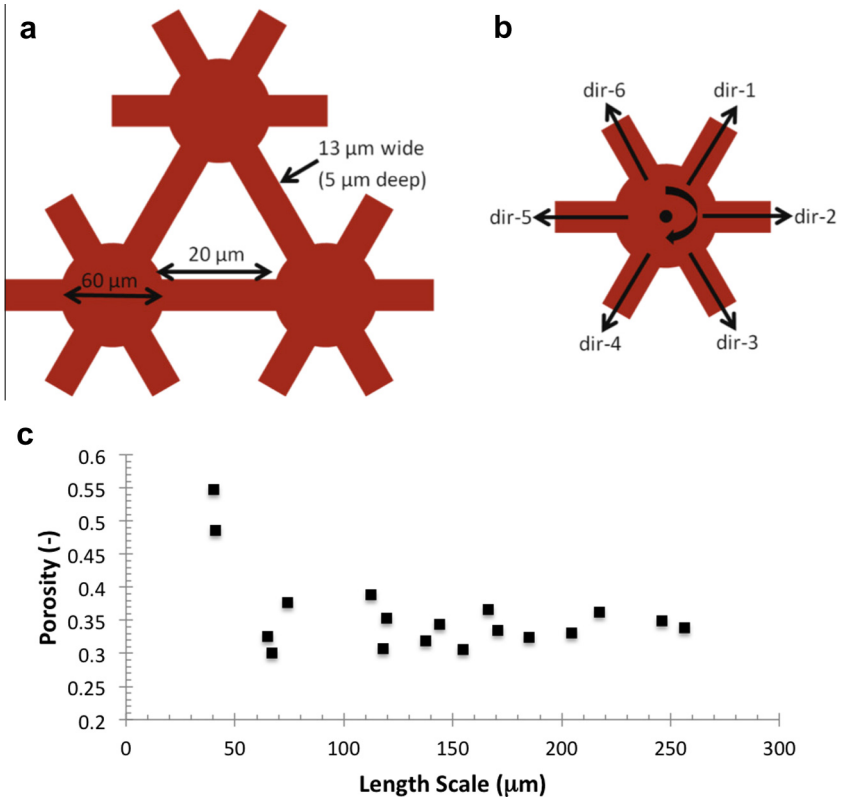

Fig. 1. Hexagonal model geometry (not to scale) used in the presented simulations and experiments (a). Line profiles used for investigating the velocity field during a Haines jump (b). REV analysis of the micromodel system, in terms or porosity (c).

Table 1
A matrix of the parameters tested with the DHD simulation tool. Case 1 (dark blue) is the baseline case, highlighted parameters are those which were increased (red) or decreased (light blue), and Case 8 (gray) is with the varied pore morphology.

Case (#)	Interfacial Tension (N/m)	Viscosity (Pa·s)	Flux (m^3/s)	Velocity (m/s)	Ca (-)	Pore Diameter (μm)	Neck Width (μm)	Depth (μm)
1	0.029	9.2E-04	1.17E-12	6.5E-04	2.08E-05	60	13	5
2	0.029	9.2E-04	1.17E-11	6.5E-03	2.08E-04	60	13	5
3	0.029	9.2E-04	4.69E-12	2.6E-03	8.32E-05	60	13	5
4	0.029	9.2E-03	1.17E-12	6.5E-04	2.08E-04	60	13	5
5	0.029	9.2E-05	1.17E-12	6.5E-04	2.08E-06	60	13	5
6	0.144	9.2E-04	1.17E-12	6.5E-04	4.16E-06	60	13	5
7	0.003	9.2E-04	1.17E-12	6.5E-04	2.08E-04	60	13	5
8	0.029	9.2E-04	2.34E-12	6.5E-04	2.08E-05	distribution	distribution	10

regions of interest within the simulation domain and experimental systems where a Haines jump is about to occur. We selected 3 regions of interest from the experimental system and then 3 from the simulation system; these were not the exact same regions. The only requirement for the region of interest was that a Haines jump must have occurred during the observed time. Prior to a Haines jump the three phase contact point remains pinned at the entrance to a pore body and the decane/water interface "bulges" into the pore body. At this point, a reference line that is normal to the interface and extends diagonally across the pore body can be drawn by visually examining an image. Once the pore entry pressure is exceeded the interface accelerates through the pore body and the movement is tracked along the reference line. From this analysis, the speed (velocity magnitude) of the oil/water interface during a Haines jump can be measured. Whereas the entire interface could be discretized and the normal velocity across the interface during a jump could be reported, we find this unnecessary since the velocity magnitude measurement is only used to validate the simulation results and to explore trends. To visualize the simulation results and thus, fluid phase velocities the magnitude of the X and Y velocity vectors were mapped to 16-bit color images. Then, velocity profiles along lines that extend outward from the center of a pore from which a Haines jump occurs are reported; therefore, the measured velocities are the phase velocities predicted from the simulation results. The direction and numbering of the line profiles are provided in Fig. 1b.

2.2. Numerical simulator

We use the method of density functional hydrodynamics (DFH), which consists of both a hydrodynamic and thermodynamic model that are coupled through the conservation laws of mass and momentum [15]. At this juncture, we only give a general description of the method and note the most relevant references since the establishment and validation of this method has progressed through a series of papers since 1995. For the hydrodynamic model, the stress tensor in the momentum equations is the sum of the viscous-stress tensor and the static-stress tensor. The first tensor determines the hydrodynamic model of the fluid, which for our case is Newtonian and therefore, we use the classical Navier–Stokes viscous-stress tensor expression. The second tensor describes static stresses in the fluids such as pressure and interfacial tension. For the thermodynamic model, Helmholtz energy is expressed as a functional of the molar density of the constitutive components (water and decane), for further details we refer to [13]. The interfacial tension between the immiscible phases is defined through the Helmholtz energy expression and the square gradients of the molar densities [15]. To couple both models, the Helmholtz energy, the first order derivatives with respect to the molar densities, and the second order spatial derivatives enter the expression for the static-stress tensor used in the momentum equation, which makes the model distinctly different from that used in the classical Navier–Stokes equations.

The DFH approach can be solved using a discretization technique applied to a digital image and therefore, the solid surface must be explicitly defined. For the simulations the following boundary conditions were used: no-slip boundary condition, impermeability condition for diffusion fluxes transverse to solid surfaces, and water-wet conditions for solid surfaces. The no-slip boundary condition does not preclude motion of interfaces over solid surfaces. Contact line motion is enabled by non-linear diffusion fluxes, which do not produce mass transfer [15]. With this approach, the moving contact line phenomenon is modeled, while the no-slip boundary condition is satisfied; examples can be found in [12]. Surface wettability was characterized by distributing Helmholtz energy surface densities over all solid surfaces. A correlated Gaussian distribution of surface energies was used to mimic the slight heterogeneity of the surface wetting properties of the borosilicate glass micromodel. The distribution parameters were adjusted to achieve the closest correspondence to the experimental observations of the menisci shapes. The resulting mean surface energy value with respect to decane was 0.019 N/m, with minimum and maximum values at 0.018 N/m and 0.020 N/m and the correlation radius was on the order of a pore size. To determine at what point which phase is present, the molar density distributions must be analyzed. Therefore, DFH does not use a phase indicator field and phase boundaries do not require any special description, i.e. phase boundaries do not need to be explicitly tracked. The position of the interface is found by post-analysis of the local molar density gradients and is defined by the sharp yet continuous transition of mixture composition from one phase to the next. A similar approach is used with the diffuse-interface method [1].

With DFH the system of equations is solved at each spatial point in a domain and the temporal progress of the system is described by the evolution of the molar densities of the constitutive components and velocities. The equations are highly non-linear and contain higher order spatial derivatives up to 4th order. Demianov et al. [12] demonstrated that this system of equations can be solved with a method, specifically designed for the DFH equations,

called Tensor-Aligned Conservative Uniform Symmetric (TACUS). TACUS is a second-order in space first-order in time explicit conservative finite-volume method, on a uniform staggered Cartesian grid, that can be parallelized and implemented on modern computer clusters. With this approach, a Direct HydroDynamic (DHD) simulator, which solves the DFH equations by the TACUS method on either CPU or GPU-based computer clusters has been developed and validated by a series of papers [13,16,17] and in a book [12]. Additionally, the DHD simulator has been used to model various pore-scale multiphase flow mechanisms [32].

From a high-level view, for the situation of two-phase immiscible flow, one can consider the DFH simulator as a method to model pore scale (Navier-) Stokes flow with moving interfaces. From a scaling analysis perspective one would arrive at a very similar set of scaling groups as the pore scale definitions in [28]. However the computational domain covers multiple individual pores and in that sense the computation also covers dynamic length scales defined through the flow and the formation of oil clusters even though these lengths are not explicitly part of the governing equations.

To model the experiments with the DHD simulator, the hexagonal geometry (including the pattern depth) shown in Fig. 1 was digitized into a 3D volume and then repeated as a 6 by 10 grid to represent the micromodel network used in the experiments. A uniform grid of $1231 \times 1067 \times 10$ cubic cells was used for Cases 1 through 7 and a uniform grid of $2246 \times 738 \times 17$ cubic cells was used for Case 8 since the micromodel depth and network dimensions were slightly different for the Gaussian distribution of pore bodies and necks. For all Cases, the length of a cell was 0.65 μm; grid refinement studies can be found in Demianov et al. [12].

In the following text, the boundary conditions are explained from the perspective as if the micromodel chip was placed flat on a horizontal surface. The model was initially saturated with water and decane was injected along the transverse side of the model domain (right hand side) at a constant rate, as defined in Table 1. On the opposite transverse side (left hand side), the phases were allowed to flow freely to ensure no accumulation of phases. Periodic boundary conditions were used on the two lateral sides since the micromodel has a periodic design and only a section of the micromodel domain (6 by 10 pore units) is used as a simulation domain. The top and bottom sides (parallel to the table) were impermeable boundaries, which represent the top and bottom glass plates of the micromodel that contain the porous network. The simulations were initialized with 100% wetting phase saturation and non-wetting phase was injected along the constant flux boundary condition. The numerical simulations were carried out until Haines jumps were observed near the center of the model domain, and therefore multiple pores away from the model boundaries. At this point, 3 jumps were randomly selected for the measurement of interfacial velocity and comparison to experimental results.

3. Results and discussion

The results and discussion are divided into the following Section 3.1 Menisci Retraction Effect, Section 3.2 Interfacial Tension versus Viscosity, Section 3.3 Capillary Number, Section 3.4 Influence of Spatial Configuration, and Section 3.5 Zone-of-Influence and 3-phase REV. We first compare the DHD simulation results to experimental results, which not only validates the simulation data but gives additional consistency to the observation in the micromodel. We then use the DHD simulator to explore the independent influence of interfacial tension and fluid viscosity on the speed of a Haines jump, which is difficult for experiments since a change in viscosity often influences interfacial tension and vice versa. The simulation results are compared in terms of the capillary number (Eq. (1)), which evaluates how appropriate *Ca* is at describing pore-scale flow. The last parameter tested was pore morphology, the results of which demonstrate how phase spatial configuration prior to a Haines jump influences interfacial dynamics. To measure the zone-of-influence of a Haines jump we use the DHD simulator to extract the fluid velocity vectors, which is a parameter not easily extractable from micromodel experiments. The results provide criteria for defining a 3-phase REV and demonstrate over what distance a Haines jump can influence fluid velocities.

3.1. Menisci retraction effect

The transient dynamics of interfaces during pore-scale displacement of immiscible phases is often overlooked when considering validation criteria for numerical simulations. However, we find this to be an important aspect for any pore-scale modeling tool and have decided to validate the presented simulations by direct comparison to experimental results captured during the transient dynamics of a Haines jump. As shown in Fig. 2, we observe for both experimental and numerical results that during a Haines jump, when drainage occurs in the pore body, imbibition occurs in the surrounding pore neck regions. In Fig. 2, we selected only a region of interest for one Haines jump simulated in the larger model domain and one Haines jump imaged in the larger experimental domain. The selection was random and therefore, the spatial

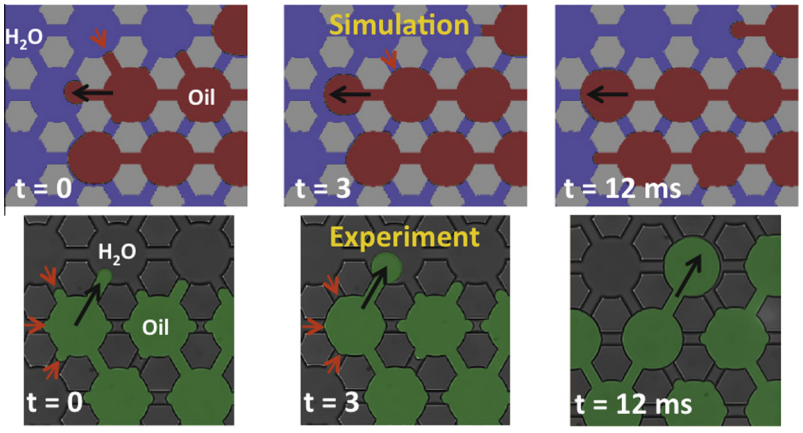

Fig. 2. Experimental and simulation results display the same cooperative pore drainage mechanism where imbibition occurs in the surround pore neck regions as drainage occurs in the pore body.

arrangement of fluid in the simulation and experiment are not identical; however, the fluid viscosities, interfacial tension, and fluid injection rate are equivalent. In this comparison we are evaluating the transient dynamics and not the exact spatial arrangement of fluids.

In an earlier publication, we explain this menisci retraction effect by the capillary pressure (P_c) difference that occurs during a Haines jump [2]. Please note that capillary pressure is defined as

$$P_c = \sigma(1/R_1 + 1/R_2) \quad (2)$$

where σ is interfacial tension (N/m) and R_1 and R_2 are the principal radii of curvature (m). This P_c difference is generated by differences in interfacial curvature (R_1 and R_2) between the meniscus in the pore body and the menisci in the pore neck regions, which is measureable from images collected during micromodel drainage experiments [2]. These results suggest that capillarity is non-local and depends not just on the entry pressure of a single pore but also the fluid spatial configuration prior to a Haines jump. For further evidence, in support of the non-locality argument, it was shown that interfacial velocities during a Haines jump are dependent on fluid spatial configuration. Therefore, the spatial configuration of the fluid should be explicitly defined and the local P_c differences across immiscible phases with moving interfaces must be respected to correctly model the dynamics of a Haines jump in a porous geometry. This appears to be the case with the presented simulations since the menisci retraction effect was observed, which gives additional validation to the observed non-local coupling.

To further evaluate the consistency between experiment and model, we measure the fluid–fluid interfacial velocities during a Haines jump from the simulation images and compare these values to experimental data. We find that the results for the simulation data compare well with the experimental measurements (Fig. 3). For both the numerical and experimental results the interface accelerates for the first 1/3 time step and then decelerates during the duration of the Haines jump. As observed in our previous work, pore drainage events occur at an intrinsic time scale that is independent of bulk flow rate. A similar trend is demonstrated with the simulation data, where the measured interfacial velocities are independent of increasing injection rate; in Fig. 3, the injection rate is represented by capillary number. These results suggest that DHD is correctly capturing the transient dynamics of the capillary-viscous regime, which is necessary for modeling multiphase flow at the pore-scale. During multiphase flow, a large scale pressure gradient is applied over the extent of the system (model domain, experimental system, or field application), while transient pressure gradients exist over a shorter length scale within the capillary dispersion zone and are caused by topological changes of the nonwetting phase. We are interested in these transient pressure gradients that from a pressure reading point of view, during core flooding or similar macroscopic studies, may appear as noise rather than displacement effects. Our results from Armstrong and Berg [2], suggest that these transient pressure gradients exist over the time scale of a Haines jump and extend over the length scale of multiple pores. Therefore, to study the transient gradients pore-scale simulations that correctly capture the dynamics of a Haines jump are required.

3.2. Interfacial tension versus viscosity

We want to study the time scale over which the transient pressure gradients exist because this sets a fundamental characteristic time scale for immiscible displacement. To better understand this time scale, we analyzed Haines jumps for a range of different fluid viscosities and interfacial tensions using the DHD simulator. The fluid parameters tested are presented in Table 1. By measuring interfacial velocities during a Haines jump, we found that the time scale of an event decreases with increasing interfacial tension and increases with increasing viscosity. In Fig. 4, we present interfacial velocities for a range of nonwetting phase viscosities, which are represented by capillary number. As viscosity increases (increasing capillary number) the time scale of an event increases from 6 to 30 ms and the peak velocity reached by the fluid–fluid interface is reduced. In Fig. 5, we present the interfacial velocities for a range of interfacial tensions, which are also represented by capillary number. As interfacial tension increases (decreasing capillary number) the time scale of an event decreases. As expected, the velocity of a Haines jump (discharge rate) should be equal to the local pressure gradient times a proportionality constant that accounts for fluid conductivity, which is true for the presented data. By increasing fluid viscosity the proportionality constant that accounts for fluid conductivity would decrease resulting in a slower event, which is observed in Fig. 4. Also, by increasing interfacial tension the local pressure values in the pore body meniscus and the surrounding pore neck menisci would increase while the distance between these menisci would remain constant and thus, the magnitude of the pressure gradient increases, resulting in a faster event.

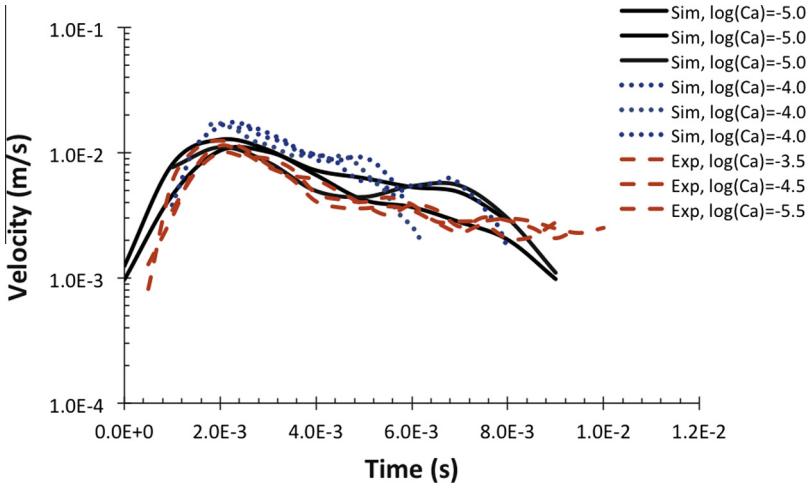

Fig. 3. Experimental and simulation results compare well for the measured speed of the oil/water interface during a Haines jump. The measured interfacial velocities for the experimental data are independent of bulk flow rate, reported as a change in capillary number (Ca). The simulation results display the same independency.

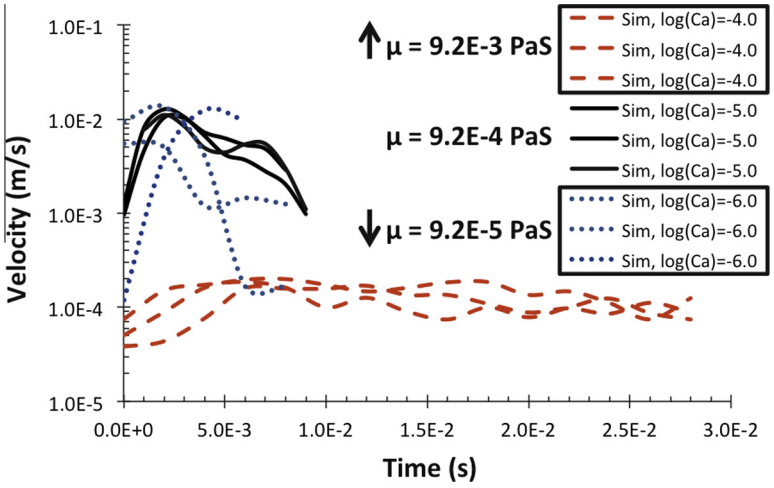

Fig. 4. Simulation results indicate that interfacial velocities are dependent on the viscosity of the invading phase, reported as a change in capillary number. For a more viscous fluid the overall time scale for a Haines jump will increase. The black boxes group results that have the same Ca.

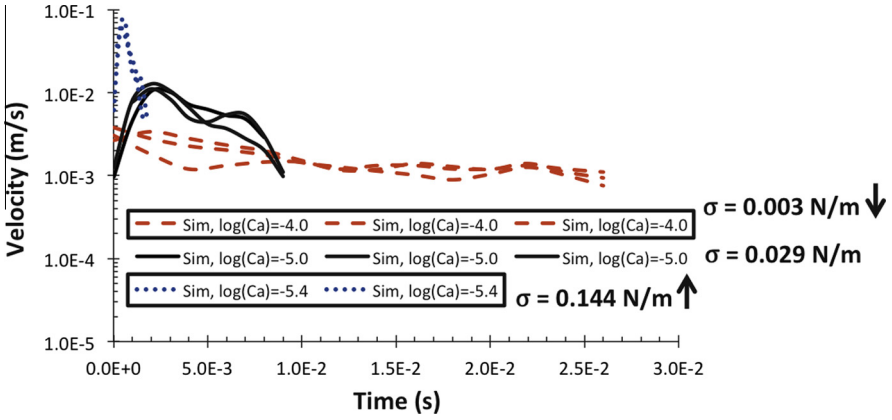

Fig. 5. Simulation results demonstrate that interfacial velocities are dependent on the interfacial tension between the two immiscible phases, reported as a change in capillary number. As interfacial tension increases the overall time scale for a Haines jump decreases. The black boxes group results that have the same Ca.

3.3. Capillary number

We find different interfacial dynamics for the same capillary number (Ca). As shown in Fig. 6, by increasing Ca by an order of magnitude from 10^{-5} to 10^{-6} via either decreasing interfacial tension or increasing nonwetting phase viscosity, significantly different interfacial velocities are measured. With either approach the interfacial velocities become less pronounced, the overall time scale of the Haines jump increases in comparison to the Baseline case ($Ca = 10^{-5}$), and the final arrangement of the oil/water interface in the drained pore are similar, i.e. the interface becomes pinned at the next pore throat. The latter observation on interfacial arrangement when a jump ceases could be caused by the uniform pore neck and body geometry since the final arrangement of the oil/water interface in the draining pore is rather constrained, also it is possible that the pinning would eventual be reduced if even lower interfacial tensions are test. However, the measured interfacial velocities are an order of magnitude different for the two cases, even though $Ca = 10^{-4}$ in both cases. This suggests the Ca is not indicative of multiphase flow at the pore-scale. As previously demonstrated, capillarity is a nonlocal process involving differences in capillary pressures over the distance of multiple pores, which creates a pressure gradient for flow to occur. However, Ca arises from an interfacial definition that balances the viscous stress at a liquid–liquid interface to the interfacial stresses at the (same) interface and therefore, does not account for longer-range effects. We demonstrated in Armstrong et al. [3] that Ca is the wrong scaling group when studying core-scale desaturation since the viscous and capillary forces act over different length scales and this appears also to be the case for pore scale fluid–fluid displacement during drainage.

3.4. Influence of spatial configuration

We also want to understand the influence of pore morphology on interfacial velocities during drainage and therefore, in this section we discuss the simulation results for Case 8 (model domain with a distribution of pore space length dimensions, see Table 1). To demonstrate this influence, we compare the maximum velocity reached by an interface during a Haines jump (V_{max}) to two different morphological parameters called *aspect ratio* and *difference*. *Aspect ratio* is the geometrical ratio between the effective width of a pore neck ($l_n = \sqrt{cross\ section\ area}$) divided by the effective length of a pore body ($l_b = \sqrt[3]{volume}$). This is a local parameter, which characterizes the local capillary forces since we consider the pore body in which the Haines jump occurs and the pore neck through which the nonwetting phase enters the pore body, see Fig. 7(a). *Difference* is l_b subtracted by l_n. However, l_n is measured from the pore neck region connected to the next neighboring pore

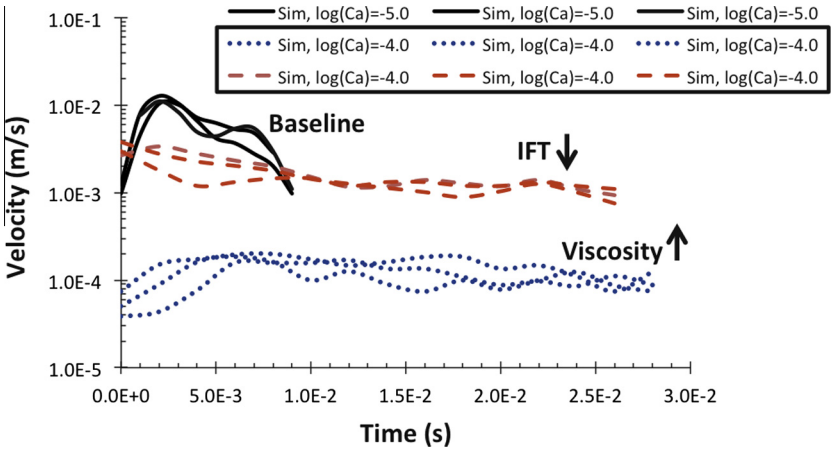

Fig. 6. Simulation results show that the capillary number (Ca) is not indicative of flow regimes at the pore-scale. For the same Ca different interfacial velocities are measured depending on whether interfacial tension is decreased or fluid viscosity is increased. The black box groups results that have the same Ca.

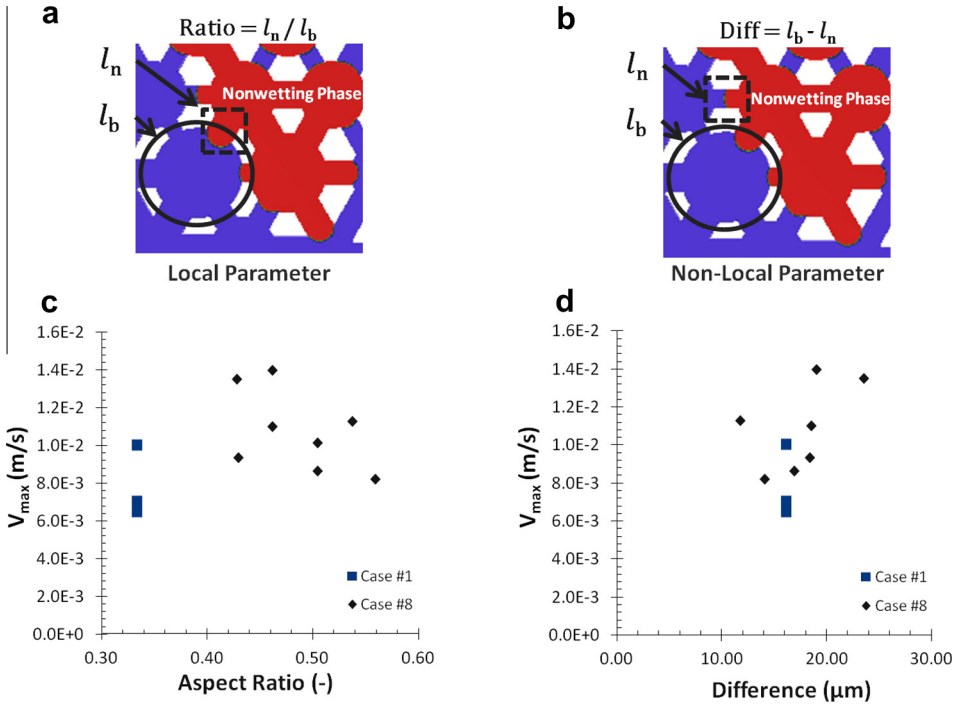

Fig. 7. *Aspect ratio* is the ratio between the effective length of a pore neck (l_n) to the effective length of a pore body (l_b , a). *Difference* is l_b subtracted by l_n (b). Simulation results show no trend between maximum interfacial velocity and pore *aspect ratio* (c); whereas, a positive trend is apparent between maximum interfacial velocity and *difference* (d).

that is connected through the nonwetting phase, see Fig. 7(b). In this way, *difference* is a nonlocal parameter that estimates the potential difference in interfacial curvature across connected phase interfaces by using a measured geometrical parameter (effective neck length) of the micromodel as a proxy to meniscus curvature. However, *difference* is not a uniquely defined parameter since there could be next-neighbor pores and so forth connected through the non-wetting phase and therefore, this parameter is only used to investigate/demonstrate the importance of capillarity (non-local capillary forces) during fluid–fluid displacement. *Aspect ratio* is a local measurement since l_n is measured from the entry region of the draining pore, whereas *difference* is a non-local parameter since l_n is measured from the pore neck of the next neighboring pore in which there is a meniscus. As shown in Fig. 7, there is no observable trend between V_{max} and *aspect ratio*, whereas there is a positive trend between V_{max} and *difference*. The positive trend only covers a small range of *difference* values because of geometrical limitations of the quasi-2D structure of the micromodel pattern; simulations in a 3D digital rock domain would be required for a larger range of *difference* values. Regardless, the results suggest that phase spatial configuration has a strong influence on interfacial dynamics during a Haines jump and thus, the overall time scale over which the transient pressure gradients exist. From a hierarchical point of view, the physical boundaries of the pore space limit the nonwetting phase spatial configuration, which limits the transient pressure differences that can occur across fluid interfaces and this dictates the speed of a Haines jump. The results suggest that a pore morphology that allows for more variability in phase spatial configuration during the nonequilibrium displacement of interfaces would result in higher speed events. If we make an argument parallel to ideas common in the field of nonequilibrium thermodynamics this could mean that the size and extent of these transient

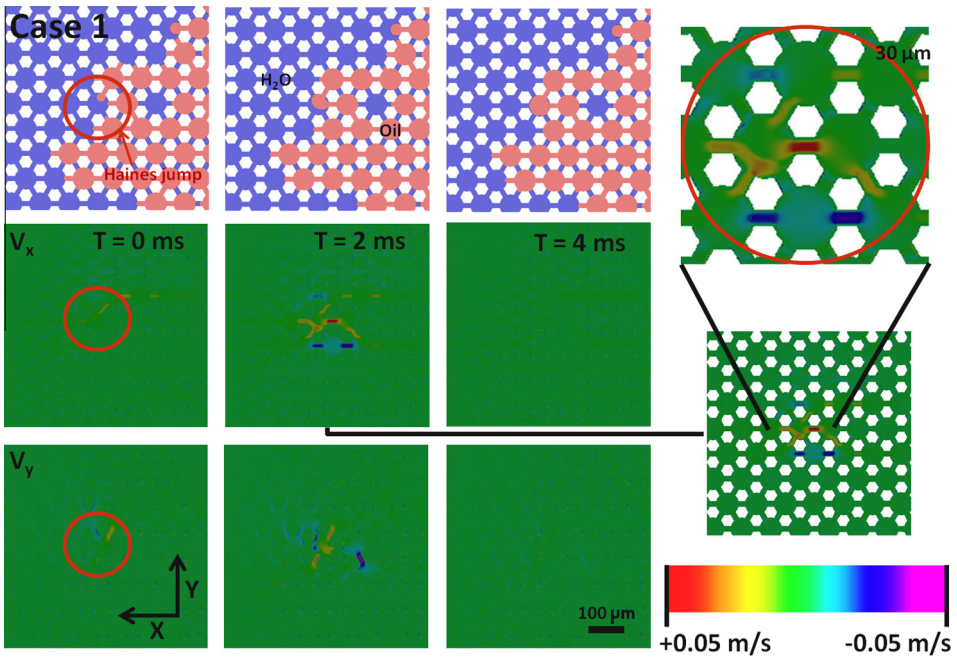

Fig. 8. Simulation results for Case 1. The start of a Haines jump is identified in the top left corner and the corresponding velocity fields (V_x, V_y) are displayed in the bottom two rows. The constant flux boundary condition used for Case 1, corresponds to an average linear pore velocity of 4.5E-4 m/s (green).

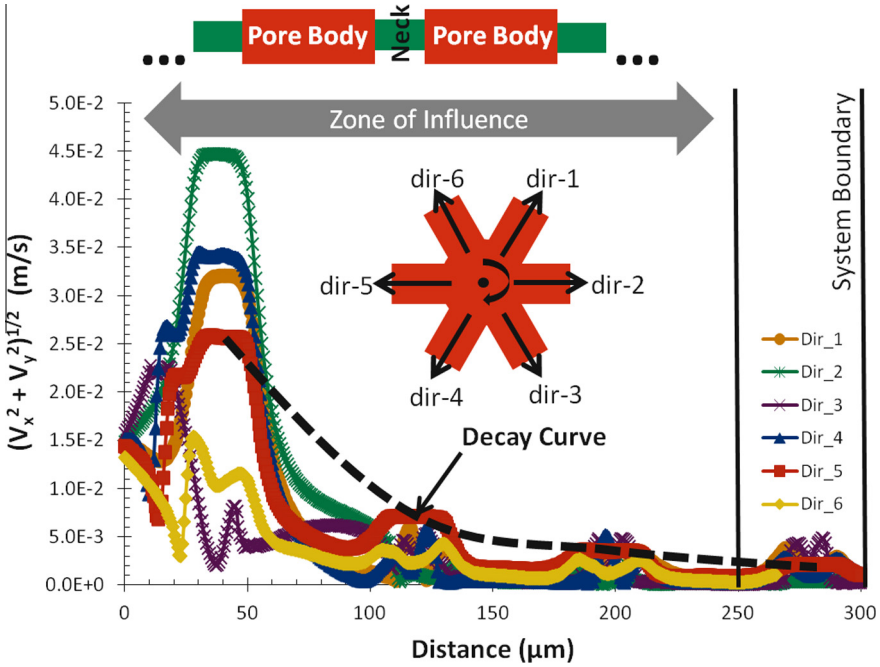

Fig. 9. Velocity profiles for Case 1. Measurements were taken along line profiles that extend outward, from the center of a pore from which a Haines jump occurs, in the 6 radial directions (Dir) that correspond to the hexagonal model geometry. Line profile measurements are reported for the maximum interfacial velocity reached during a jump. For Case 1, the results demonstrate that a Haines jump affects the velocity field at a radial distance less than 250 µm. The observed increase in phase velocity directly beyond the zone of influence is due to an expected velocity increase in the pore neck region of the micromodel.

pressure gradients are influenced by the degree of randomness in the system, which from the hierarchical point of view is limited by the pore morphology.

3.5. Zone of influence and 3-phase REV

To model pore-scale behavior and/or up-scale multiphase flow through porous media, we must consider a domain size that is large enough to capture the physics of all pore-scale mechanisms. Often a representative volume [6] is defined by measuring porosity, saturation, or specific interfacial area at static or quasi-static conditions, which is a convenient approach but likely disregards important dynamic effects. An alternative approach is to study the length scales associated with the commonly known pore-scale mechanisms since these length scales should define the lower limit of a representative volume. Therefore, we ask the question as to

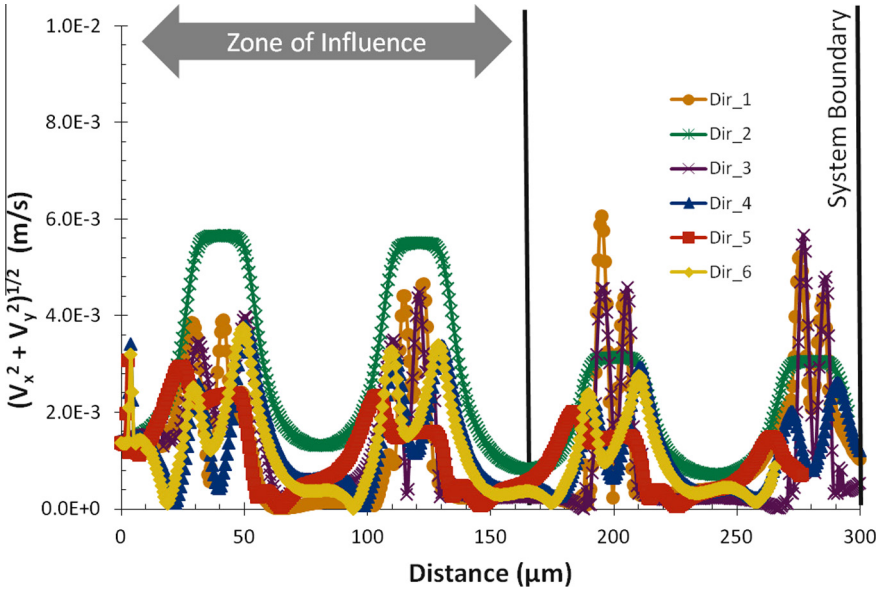

Fig. 10. Velocity profiles for Case 5. The viscosity of the nonwetting phase was increased by an order of magnitude, in respect to Case 1 (Fig. 9). By increasing the nonwetting phase viscosity, the zone of influence was decreased.

whether or not dynamic effects influence the definition of a representative volume since the parameters that are often measured (e.g. saturation and/or interfacial area) to define a representative volume are regularly measured under equilibrium conditions. To assess the length scale of a Haines jump, we have chosen to analyze the associated pore-scale velocity field and define the zone of influence as the radial distance from a Haines jump over which measured fluid velocities are greater than the average linear pore velocity (as calculated from the fluid injection rate and measured micromodel geometry). Sequential snap-shots of the phases and fluid velocities over the duration of a Haines jump are displayed in Fig. 8 (results from Case 1). During a Haines jump the measured fluid velocities in the surrounding pore regions are greater than the average linear pore velocity of 4.5E-4 m/s. In particular, the largest velocities are measured in the pore neck regions that are adjacent to the pore body in which the Haines jump occurs. For the tested cases, fluid velocities in the adjacent pore neck regions range from 6.0E-3 m/s (Case 4) to 2.3E-1 m/s (Case 6), which correspond to local Reynolds numbers of 3.4E-3 and 1.3, respectively. Case 4 had the largest nonwetting phase fluid viscosity and Case 6 had the largest interfacial tension value (see Table 1). Even though the measured velocities dissipate at regions further from the origin of the event, the high velocities are sustained for a distance greater than a single pore.

To quantify the zone of influence we measured the speed of the fluids (phase velocities) along line profiles that extend outward from the center of a pore in which a Haines jump occurs (see Fig. 1(b)). We define the zone of influence as the distance over

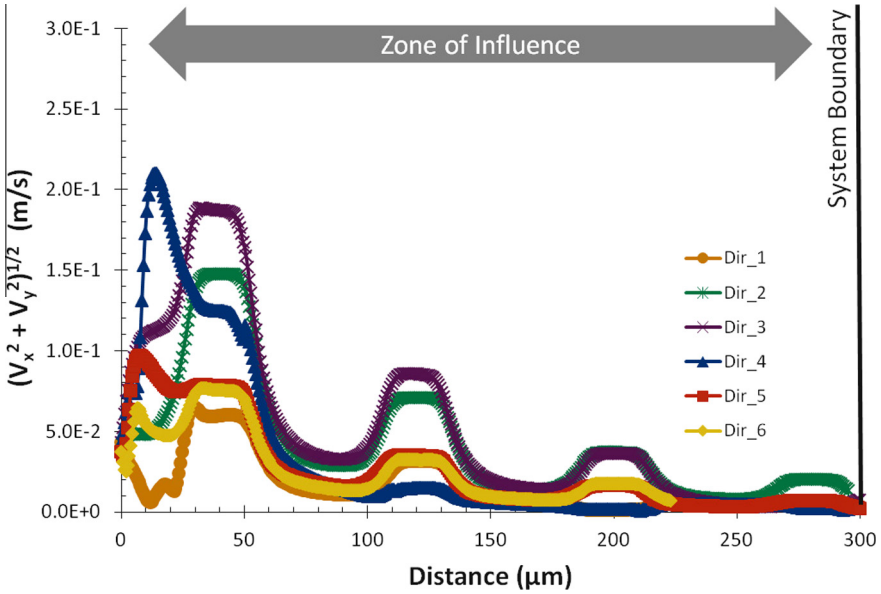

Fig. 11. Velocity profiles for Case 6. The interfacial tension between the immiscible phases was increased by 5×, in respect to Case 1 (Fig. 8). The zone of influence appears to extend across the entire simulation domain. The longest distance from the reported Haines jump to the model boundary is ~300 μm and the measured pore velocity at this distance is than the average linear pore velocity of 4.5E-4 m/s, as calculated from the constant flux boundary condition.

which the measured phase velocities are greater than the average pore velocity (Darcy velocity measured from the injection flux). The phase velocity measurements are taken when the interfacial velocity during a Haines jump reaches V_{max}; however, the interfacial velocities are not reported in the following figures. The results are presented in Figs. 9–11, which correspond to Case 1, 5, and 6, respectively. The presented Cases correspond to the largest (Case 6), intermediate (Case 1), and lowest (Case 4) measured velocities, which evaluates the range of potential values for the zone of influence within the parameters tested (see Table 1). Figs. 9–11 demonstrate that the zone of influence ranges from 175 μm to > 300 μm in radius (measured velocity > average pore velocity). Considering that the modeled domain is 800 μm by 694 μm then a Haines jump that occurs in the middle of the domain would influence the velocity field across the entire model. Therefore, the Haines jump is not independent of the boundary conditions for a domain of 8 by 8 pores. Also, Haines jumps across the displacement front are not independent local events. On the contrary, within the zone of influence, interference between simultaneous Haines jumps would occur and single events could trigger sequential events a similar observation was presented by [36]. Additionally, Ferrari and Lunati [20] have recently demonstrated that fluid–fluid displacement events should be considered when up-scaling multiphase flow since in their pore scale simulations inertial effects influenced the work done by external forces.

When performing pore-scale simulations the time and length scales for a Haines jump must be considered in detail to correctly capture system dynamics. The typical minimum length dimension for an REV in porous rock samples is often defined as 10 grains [6]. However, Bear's REV concept is based on a correlation length and since our geometry is homogenous the correlation length scale is only 250 μm or approximately 1.5 of the pore unit presented in Fig. 1(a). For example, a meaningful measurement of porosity could be computed from 1.5 pore units (see Fig. 1(c)). However, the observed zone of influence due to dynamic effects was measured to be as large at 300 μm in radius, which results in an observation window of approximately 600 μm, i.e. 350 μm larger than the REV defined in terms of porosity. This provides insight that there is another length scale defined by immiscible displacement and that, in this particular case, the length scale is larger then the REV as would be defined by Bear [6]. How this works in a 3D porous medium with a broader pore size distribution remains to be seen. Also, how this length scale interferes with intrinsic correlation lengths of the static porous medium remains to be investigated in the future. However, any simulator tool must provide fine temporal resolution (~milliseconds) and be able to handle volumes greater than 8 by 8 pores. Also, flow behavior within 4 pores from the boundary should be disregarded. Therefore, to observe a 10 by 10 pore system, an 18 by 18 pore system should be simulated. While these estimates are likely less for a 3D system, we remain on the conservative side by making our estimate using results from a 2D system with the largest measured zone of influence. The relationship between the time and length scales for the transient pressure gradients is interesting since the length scale is inversely proportional to the time scale. As the local pressure gradients become steeper the overall time scale at which the system relaxes to equilibrium decreases; however, the length scale over which the pressure gradient influences the flow field increases. This means that for pore-scale simulations as interfacial tension increases the REV size would also increase, and conversely for increasing fluid viscosity. This would also impact how either the temporal or spatial averages of a system should be considered, which may not necessarily be the same. For a low capillary number system, where low flow rate compensates for high interfacial tension, the frequency and time scale over which the local pressure gradients exist would be low and average-out over long enough time. However, the spatial average taken at the moment of an event would not necessarily average-out depending on the volume of space analyzed. Therefore, one approach for determining a representative volume would be to check if the spatial and temporal averages converge. This would mean that an 8 by 8 pore system would be required to correctly simulate a single Haines jump in the center of the domain but this would not necessarily be a representative volume. Rather, a volume large enough for the pore velocity to average to the same value as the temporal average of the pore velocities, for a given event frequency, would be required.

4. Conclusions

During the drainage of a porous rock a capillary dispersion zone is observed, over which wetting phase saturation is reduced. The pressure gradient applied over the extent of the porous rock drives the macro-scale movement of the capillary dispersion zone forward. However, local transient pressure gradients within the capillary dispersion zone drive the progression of the dispersion zone. These transient pressure gradients occur during geometrical changes of interfaces, which create moments when the interfacial curvature of fluid–fluid interfaces is not constant. Such a situation occurs during Haines jumps: as a nonwetting phase invades a less geometrically constrained region of the pore space. The duration of a Haines jump and distance over which fluid velocities are influenced by a jump set characteristic length and time scales for the transient pressure gradients. We have shown that these length and time scale are inversely proportional and are influenced by intrinsic fluid parameters; such as, interfacial tension and nonwetting phase viscosity, and also by pore morphology. We measure significantly different interfacial dynamics at the same capillary number depending on whether viscosity is increased or interfacial tension is decreased, which indicates that Ca is inadequate at describing fluid–fluid displacement at the pore-scale. The zone of influence associated with a Haines jump was found to exist over a distance of multiple pores and thus is much larger than the correlation length for the homogenous model pattern. This sets a lower limit for the size of a representative volume for dynamic conditions, i.e. when considering large local velocities that occur during Haines jumps, and demonstrates that this limit is larger than what would be measured by considering only the pore space geometry (e.g. porosity). By considering the frequency of Haines jumps for a given system and the amount of fluid–fluid interfacial area within the capillary dispersion zone the average distance between jumps could be estimated, as suggested by Mohanty [37]. If this distance is less than the characteristic length scale for a Haines jump then the high speed fluid velocities associated with a Haines jump would not necessarily average-out when considering regions within the capillary dispersion zone. Overall, for a pore-scale simulation to capture the dynamic effects of fluid–fluid displacement, we suggest the following simulation criteria: a domain size large enough to include the zone-of-influence and represent differences in curvature over the surrounding fluid–fluid interfaces, a temporal resolution fine enough to capture millisecond events, and a simulation time long enough for the temporal and spatial averages of pore-scale parameters to converge.

Acknowledgment

Katie Humphry and Rob Neiteler are gratefully acknowledged for the design of the micromodel pattern and micromodel holder, respectively. Additionally, we would like to acknowledge Open Source Physics, which is supported in part by the National Science Foundation Grants DUE-0126439 and DUE-0442481 and Douglas Brown for developing the Tracker Video Analysis and Modeling

Tool. We also thank Apostolos Georgiadis, Oleg Dinariev, Sergey Safonov, and Katie Humphry for valuable discussions regarding capillarity and performing the internal review of the paper. Lastly, we would like to thank the three anonymous reviewers for assisting with the evaluation of this manuscript.

References

[1] Anderson DM, McFadden GB. Diffuse-interface methods in fluid mechanics. Ann Rev Fluid Mech 1998;30:139–65. http://dx.doi.org/10.1146/annurev.fluid.30.1.139.

[2] Armstrong RT, Berg S. Interfacial velocities and capillary pressure gradients during Haines jumps. Phys Rev E 2013;88(4). http://dx.doi.org/10.1103/PhysRevE.88.043010.

[3] Armstrong RT, Georgiadis A, Ott H, Klemin D, Berg S. Critical capillary number: desaturation studied with fast X-ray computed microtomography. Geophys Res Lett 2014;41:1–6. http://dx.doi.org/10.1002/2013GL058075.

[4] Armstrong RT, Porter ML, Wildenschild D. Linking pore-scale interfacial curvature to column-scale capillary pressure. Adv Water Res 2012;46:55–62. http://dx.doi.org/10.1016/j.advwatres.2012.05.009.

[5] Avraam DG, Payatakes AC. Flow regimes and relative permeabilities during steady-state two-phase flow in porous media. J Fluid Mech 1995;293:207–36. http://dx.doi.org/10.1017/S0022112095001698.

[6] Bear J. Dynamics of Fluids in Porous Media. Dover Publications Inc.; 1988. ISBN 0486131807.

[7] Berg, S, Ott, H, Klapp SA, Schwing A, Neiteler R, Brussee N, et. al., Real-time 3D imaging of Haines jumps in porous media flow. Proceedings of the National Academy of Sciences (PNAS) 110 (10), 3755–3759, doi: http://dx.doi.org/10.1073/pnas.1221373110.

[8] Blunt MJ. Flow in porous media – pore-network models and multiphase flow. Current Opinion Colloid Interface Sci 2001;6(3):197–207. http://dx.doi.org/10.1016/S1359-0294(01)00084-X.

[9] Blunt MJ, Bijeljic B, Dong H, Gharbi O, Iglauer S, Mostaghimi P, Paluszny A, Pentland C. Pore-scale imaging and modeling. Adv Water Res 2013;51:197–216. http://dx.doi.org/10.1016/j.advwatres.2012.03.003.

[10] Cheng JT, Pyrak-Nolte LJ, Nolte DD, Giordano NJ. Linking pressure and saturation through interfacial areas in porous media. Geophys Res Lett 2004;31(8). http://dx.doi.org/10.1029/2003GL019282.

[11] Chen S, Doolen D. Lattice boltzmann method for fluid flow. Ann Rev Fluid Mech 1998;30:329–64. http://dx.doi.org/10.1146/annurev.fluid.30.1.329.

[12] Demianov A, Dinariev O, Evseev N. Introduction to the Density Functional Method in Hydrodynamics. Moscow: Fizmatlit; 2014. 978-9221-1539-1, [in English], ISBN 978922115391.

[13] Demianov A, Dinariev O, Evseev N. Density functional modeling in multiphase compositional hydrodynamics. Canadian J Chem Eng 2011;89(2):206–26. http://dx.doi.org/10.1002/cjce.20457;
Demyanov A, Dinariev O. Modeling of multicomponent multiphase mixture flows on the basis of the density functional method. Fluid Dyn 2004;39(6):933–44. http://dx.doi.org/10.1007/s10697-004-0009-9;
Demyanov A, Dinariev O. Application of the density-functional method for numerical simulation of flows of multispecies multiphase mixtures. J Appl Mech Tech Phys 2004;45(5):670–8. http://dx.doi.org/10.1023/B:JAMT.0000037965.14064.a9.

[14] DiCarlo DA, Cidoncha JIG, Hickey C. Acoustic measurements of pore-scale displacements. Geophys Res Lett 2003;30:17. http://dx.doi.org/10.1029/2003GL017811.

[15] Dinariev O. A hydrodynamic description of a multicomponent multiphase mixture in narrow pores and thin layers. J Appl Math Mech 1995;59(5):745–52. http://dx.doi.org/10.1016/0021-8928(95)00087-9.

[16] Dinariev O, Evseev N. Description of the flows of two-phase mixtures with phase transitions in capillaries by the density-functional method. J Eng Phys Thermophys 2005;78(3):474–81. http://dx.doi.org/10.1007/s10891-005-0083-9;
Dinariev O, Evseev N. Description of viscous-fluid flows with a moving solid phase in the density-functional theory. J Eng Phys Thermophys 2007;80(5):70–7. http://dx.doi.org/10.1007/s10891-007-0123-8;
Dinariev O, Evseev N. Application of density-functional theory to calculation of flows of three-phase mixtures with phase transitions. J Eng Phys Thermophys 2007;80(6):1247–55. http://dx.doi.org/10.1007/s10891-007-0161-2.

[17] Dinariev O, Evseev N. Modeling of surface phenomena in the presence of surface-active agents on the basis of the density-functional theory. Fluid Dyn 2010;45(1):85–95. http://dx.doi.org/10.1134/S0015462810010102.

[18] Dullien FAL. Porous Media: Fluid Transport and Pore Structure. 2nd ed. Academic Press; 1979. ISBN 0-12-223651-3.

[19] Fatt I. The network model of porous media I. capillary pressure characteristics. Trans AIME 1956;207:144–203.

[20] Ferrari A, Lunati I. Inertial effects during irreversible meniscus reconfigurations in angular pores. Adv Water Res 2014;74:1–13. http://dx.doi.org/10.1016/j.advwatres.2014.07.009.

[21] Gray WG, Miller CT. Thermodynamically constrained averaging theory approach for modeling flow and transport phenomena in porous medium systems: 1. motivation and overview. Adv Water Res 2005;28:161–80. http://dx.doi.org/10.1016/j.advwatres.2004.09.005.

[22] Gray WG, Miller CT. Thermodynamically constrained averaging theory approach for modeling flow and transport phenomena in porous media systems: 8. Interface and common curve dynamics. Adv Water Resour 2010;33(12):1427–43. http://dx.doi.org/10.1016/j.advwatres.2010.01.010.

[23] Gray WG, Miller CT. TCAT analysis of capillary pressure in non-equilibrium, two-fluid-phase, porous medium systems. Adv Water Res 2011;34:770–8. http://dx.doi.org/10.1016/j.advwatres.2011.04.001.

[24] Haines WB. Studies in the physical properties of soil. V. the hysteresis effect in capillary properties, and the modes of moisture distribution associated therewith. J Agr Sci 1930;20(97):97–116. http://dx.doi.org/10.1017/S002185960008864X.

[25] Hassanizadeh SM, Gray WG. Mechanics and thermodynamics of multiphase flow in porous media including interphase boundaries. Adv Water Res 1990;13(4):169–86. http://dx.doi.org/10.1016/0309-1708(90)90040-B.

[26] Hassanizadeh SM, Gray WG. Thermodynamic basis of capillary-pressure in porous-media. Water Resour Res 1993;29(10):3389–405. http://dx.doi.org/10.1029/93WR01495.

[27] Held RJ, Celia MA. Modeling support of functional relationships between capillary pressure, saturation, interfacial area and common lines. Adv Water Resour 2001;24:325–43. http://dx.doi.org/10.1016/S0309-1708(00)00060-9.

[28] Hilfer R, Oren PE. Dimensional analysis of pore scale and field scale immiscible displacement. Transp Porous Media 1996;22:53–72. http://dx.doi.org/10.1007/BF00974311.

[29] Hilpert M. Velocity-dependent capillary pressure in theory for variably-saturated liquid infiltration into porous media. Geophys Res Lett 2012;39:L06402. http://dx.doi.org/10.1029/2012GL051114.

[30] Joekar-Niasar V, Hassanizadeh SM, Leijnse A. Insights into the relationship among capillary pressure, saturation, interfacial area and relative permeability using pore-network modeling. Transp Porous Media 2008;74:201–19. http://dx.doi.org/10.1007/s11242-007-9191-7.

[31] Karadimitriou NK, Musterd M, Kleingeld PJ, Hassanizadeh SM, Joekar-Niasar V. On the fabrication of PDMS micro-models by rapid prototyping and their use in two-phase flow studies. Water Resour Res 2013;49(4):2056–67. http://dx.doi.org/10.1002/wrcr.20196.

[32] Koroteev D, Dinariev O, Evseev N, Klemin D, Nadeev A, Safonov S, Gurpinar O, Berg S, van Kruijsdijk C, Armstrong RT, Myers MT, Hathon L, de Jong H. Direct Hydrodynamic Simulation of Multiphase Flow in Porous Rock. California, USA: Napa Valley; 2013. SCA2013-014.
Koroteev D, Dinariev O, Evseev N, Klemin D, Safonov S, Gurpinar O, Berg S, van Kruijsdijk C, Myers M, Hathon L, de Jong H. Application of digital rock technology for chemical EOR screening, SPE-165258, 2013.

[33] Lake LW. Enhanced Oil Recovery. ISBN: Prentice Hall; 1989. ISBN 0132816016.

[34] Lenormand R, Zarcone C, Sarr A. Mechanisms of the displacement of one fluid by another in a network of capillary ducts. J Fluid Mech 1989;135:337–53. http://dx.doi.org/10.1017/S0022112083003110.

[35] Lunati I, Jenny P. Multiscale finite-volume method for compressible multiphase flow in porous media. J Comput Phys 2006;216(2):616–36. http://dx.doi.org/10.1016/j.jcp.2006.01.001.

[36] Moebius F, Or D. Interfacial jumps and pressure bursts during fluid displacement in interacting irregular capillaries. J Colloids Interface Sci 2012;377:406–15. http://dx.doi.org/10.1016/j.jcis.2012.03.070.

[37] Mohanty KK, Davis HT, Scriven LE. Physics of oil entrapment in water-wet rock. SPE Reser Eng 1987:113–28. SPE 9406.

[38] Morrow N. Physics and thermodynamics of capillary. Ind Eng Chem 1969:32–56. Flow Through Porous Media Symposium.

[39] Nordbotten JM, Celia MA, Dahle HK, Hassanizadeh SM. On the definition of macroscale pressure for multiphase flow in porous media. Water Resour Res 2008;44:6. http://dx.doi.org/10.1029/2006WR005715.

[40] Porter ML, Schaap MG, Wildenschild D. Lattice-Boltzmann simulations of the capillary pressure-saturation-interfacial area relationship for porous media. Adv Water Res 2009;32(11):1632–40. http://dx.doi.org/10.1016/j.advwatres.2009.08.009.

[41] Porter ML, Wildenschild D, Grant G, Gerhard JI. Measurement and prediction of the relationship between capillary pressure, saturation, and interfacial area in a NAPL-water-glass bead system. Water Resour Res 2010;46:W08512. http://dx.doi.org/10.1029/2009WR007786.

[42] Reeves PC, Celia MA. A functional relationship between capillary pressure, saturation and interfacial area as revealed by a pore-scale network model. Water Res Res 1996;32(8):2345–58. http://dx.doi.org/10.1029/96WR01105.

[43] Van Winden JF, Suijberbuijk B, Joekar-Niasar V, Brussee N, van der Linde H, Marcelis A, Coorn A, Pieterse S, Ganga K, Al-Qarshubi I. The critical parameters for low salinity flooding: the relative importance of crude oil, brine, and rock, IOR 2013-From Fundamental Science to Deployment, 2013.

[44] Weitz DA, Stokes JP, Ball RC, Kushnick AP. Dynamic capillary pressure in porous media: origin of the viscous-fingering length scale. Phys Rev Lett 1987;59:26.